



Assessment of air management strategies to improve the transient response of advanced gasoline engines operating under high EGR conditions

José Galindo^a, Héctor Climent^a, Joaquín de la Morena^a, David González-Domínguez^{a,*}, Stéphane Guilain^b

^a CMT Motores Térmicos, Universitat Politècnica de València, 46022, Valencia, Spain

^b Renault Nissan Mitsubishi, 91510, Lardy, France

ARTICLE INFO

Keywords:

Gasoline engine
EGR
Transient operation
Engine 1D simulation

ABSTRACT

Advanced gasoline engines may lead the medium-term future of the passenger vehicle market, working in conventional and hybrid powertrains. Downsizing with turbocharging is the most extended way to improve fuel economy in gasoline engines. It is also proven that exhaust gas recirculation (EGR) reduces fuel consumption, but extracting the maximum benefit from EGR requires operating with high EGR rates. This fact can compromise the transient engine operation due to the greater turbocharger dependence. This research evaluates the EGR influence on the transient response of a turbocharged gasoline engine and, mainly, the potential of three air management strategies to accelerate the said response. Tip-in maneuvers at 1500 rpm (6–12 bar BMEP) were tested and simulated to this end. The three strategies are: reducing the EGR dilution by closing the EGR valve simultaneously with the throttle opening, using a pressurized air tank (PAT), and installing an electric supercharger at the compressor outlet in series. Engine tests show that the torque response time with EGR is 2-s slower than without EGR. 1D modeling results reveal that: the PAT connected to the intake manifold provides the fastest response, and the electric supercharger guarantees an excellent tradeoff between fuel consumption and torque response.

1. Introduction

Compliance with emission regulations clearly determines the activity of automotive companies, forcing them to develop greener and more efficient cars. Most manufacturers are increasingly opting for powertrain electrification to reduce greenhouse gases. Battery electric vehicles are the main alternative to fossil fuels. However, they still have significant drawbacks, such as limited driving ranges, long charging times and lack of charging points, high production costs, polluting battery manufacturing, and uncertain benefits in the well-to-wheel CO₂ emissions [1,2]. In this scenario, advanced spark-ignition (SI) engines working in hybrid electric powertrains have become one of the most competitive solutions for passenger cars, achieving very good results in terms of fuel economy without excessively increasing the complexity and costs [3,4]. The potential of hybridization with SI engines (usually fueled with gasoline) mainly lies in avoiding the engine operation at low loads, where fuel efficiency is poor [5,6].

Focusing on SI gasoline engines, the most usual strategy to reduce

fuel consumption is downsizing with direct fuel injection, while turbocharging is required to maintain peak power [7,8]. Research studies have evidenced that downsizing with direct injection increases the compression ratio and reduces pumping and friction losses, leading to fuel improvements of over 25% [9,10]. Another interesting strategy is exhaust gas recirculation (EGR), whose benefits in fuel economy have been widely proved [11,12]. Luján et al. [13] and Siokos et al. [14] stated that cooled low-pressure EGR provided up to 5% fuel saving at partial loads because of a: reduction in heat losses, lower throttling, and lesser knocking tendency resulting in a better combustion phasing. EGR enables an additional fuel improvement at high engine speeds and loads, avoiding fuel enrichment to control the exhaust gas temperature at the turbine inlet [15].

Extracting the full EGR potential in SI engines requires operating with high EGR levels [12,16], but it is subject to some issues. An excessive dilution of the air-fuel mixture in the combustion chamber may lead to undesirable misfires. On this matter, ignition systems have been improved in the last years to increase the EGR tolerance. Shimura et al. [17] and Pilla et al. [18] declared that high-energy dual-coil

* Corresponding author. CMT-Motores Térmicos, Universitat Politècnica de València, Camino de Vera s/n, 46022, Valencia, Spain.

E-mail address: dagondo1@mot.upv.es (D. González-Domínguez).

<https://doi.org/10.1016/j.energy.2022.125586>

Received 26 July 2022; Received in revised form 19 September 2022; Accepted 24 September 2022

Available online 28 September 2022

0360-5442/© 2022 Elsevier Ltd. All rights reserved.

Acronyms

AMF	air mass flow
ANN	artificial neural network
BMEP	brake mean effective pressure
BSFC	brake specific fuel consumption
CAD	crank-angle degrees
ECU	engine control unit
EGR	exhaust gas recirculation
EM	electric motor
FMEP	friction mean effective pressure
FWC	four-way catalyst
IMEP	indicated mean effective pressure
PAT	pressurized air tank
SI	spark ignition
VGT	variable geometry turbine
VVT	variable valve timing
WLTP	Worldwide harmonized Light vehicle Test Procedure

ignition systems enabled EGR rates of up to 30%. However, despite these advances, high EGR operation through low-pressure systems can compromise combustion stability under transient conditions, mainly due to the long transport delays inherent to such EGR systems [19]. Siokos et al. [20] and Galindo et al. [21] reported the occurrence of misfires under high EGR conditions during aggressive load-decrease maneuvers (tip-outs). They concluded that the slow EGR evacuation from the intake line (compared to the fast load reduction) and the lower EGR tolerance at the final tip-out operating point were the causes of misfiring.

The use of high EGR levels in downsized SI engines also involves a greater dependence on the turbocharger, given that higher pressure values at the intake manifold are required to reach a specific load. This may be particularly critical for acceleration and load-increase maneuvers because turbocharger lag becomes much more relevant, resulting in slow engine response. Hence the paper is devoted to studying the behavior of a downsized turbocharged SI gasoline engine with variable geometry turbine (VGT) technology under high EGR conditions during a tip-in maneuver. This transient maneuver refers to the engine load increase at a quasi-constant speed that happens in the first moments after the driver suddenly presses the accelerator. The main contribution of the present work is twofold: determining the impact of high EGR operation on the transient engine response and evaluating the application of air management strategies to improve the said response. Such strategies are three: reducing EGR by quickly closing the EGR valve simultaneously with the throttle opening; using a small tank of pressurized air that can be connected to either the intake manifold [21,22] or the compressor inlet; and installing an electric supercharger [23,24] at the compressor outlet in series. Effective management of the transient engine performance is essential to operate with EGR rates close to the dilution tolerance and thus extract the full EGR potential to reduce fuel consumption. Therefore, the research contribution may be very useful for CO₂ emission reduction in both conventional and hybrid vehicles. Besides, the management of transient maneuvers is even more critical for manufacturers since the adoption of new certification procedures, such as the Worldwide harmonized Light vehicle Test Procedure (WLTP) and Real Driving Emissions.

A methodology that combines experimental and modeled tip-ins at 1500 rpm from 6 to 12 bar BMEP is followed in this study. Engine tests are used to analyze the EGR influence on transient operation, validate the engine model performance, and assess the EGR reduction strategy. The pressurized air tank and electric supercharger systems are investigated via 1D modeling. It should be remarked that both torque response and fuel economy criteria are considered to evaluate the three air

management strategies. The tip-in operating conditions mentioned above were selected for two reasons. Firstly, the initial working point (6 bar BMEP and 1500 rpm) is quite relevant in the WLTP driving cycle. Secondly, there is a significant difference between operating with and without EGR at the final tip-in point. Turbocharging is almost not required without EGR to reach 12 bar BMEP, while the VGT mechanism must be closed above 80% with EGR.

The paper is structured as follows: the experimental set-up is explained in Section 2, the 1D engine model is described in Section 3, the results and discussion are presented in Section 4, and the conclusions are provided in Section 5.

2. Experimental set-up

The experimental facility and instrumentation used in this work are described in two previous studies [21,25]. A downsized (1.3 l) turbocharged direct injection SI gasoline engine with variable valve timing (VVT), four-way catalyst (FWC), and VGT technologies is utilized. Table 1 shows the main engine's attributes. The VVT system enables the variation of the intake and exhaust camshaft timings in a range of 40 crank-angle degrees (CAD) without modifying the valve lift or opening duration. The FWC device consists of a conventional three-way catalyst followed by a gasoline particulate filter, and the VGT allows for a maximum boost pressure of 2.5 bar. Besides, a low-pressure EGR system has been appended to the original engine. The EGR loop is composed of the EGR valve, a water-to-air intercooler, and a T-shape flow splitter to extract the exhaust gases at the FWC outlet. An additional valve is placed in the intake path upstream of the EGR junction. This valve, named "intake flap", is required to operate with high EGR rates. All these systems and devices are represented in the schematic engine's layout provided in Fig. 1.

The engine is installed and fully instrumented in a dynamic test rig with an AVL AFA 200/4-8EU dynamometric brake controlled through the AVL PUMA software. This software is used to regulate the engine speed and load, and to acquire the pressure and temperature values in relevant engine parts, air and fuel mass flows, turbocharger speed, and engine raw emissions, all with a 20 Hz acquisition frequency. The location of the temperature (K-type thermocouples) and pressure (Kistler 4260A piezoresistive type transmitters) sensors is shown in Fig. 1. The air and fuel mass flows and turbocharger speed are registered using AVL FLOWSONIX, AVL 733S, and MICRO-EPSILON DZ140. In addition, two gas analyzers are employed: the HORIBA MEXA-ONE to measure raw NO_x, CO₂, CO, and HC emissions, and the Cambustion NDIR500 to provide fast transient CO₂ measurements at the intake manifold. The EGR rate is estimated by applying Eq. (1) according to Ref. [26]:

$$EGR [\%] = \frac{[CO_2]_{intake} - [CO_2]_{ambient}}{[CO_2]_{exhaust} - [CO_2]_{ambient}} \cdot 100 \quad (1)$$

where the intake ($[CO_2]_{intake}$) and exhaust ($[CO_2]_{exhaust}$) mole fractions of carbon dioxide are measured at the intake manifold and turbine outlet, respectively. The $[CO_2]_{ambient}$ represents the ambient mole fraction of CO₂.

Table 1
Engine's attributes.

Attribute	Description
Technology	4-stroke GTDI
Displacement	1300 cc
Compression ratio	10:1
Number of cylinders	4
Camshaft system	Variable valve timing
Total number of valves (intake/ exhaust)	8/8
Turbocharger	Water-cooled with variable geometry turbine
Aftertreatment system	Four-way catalyst

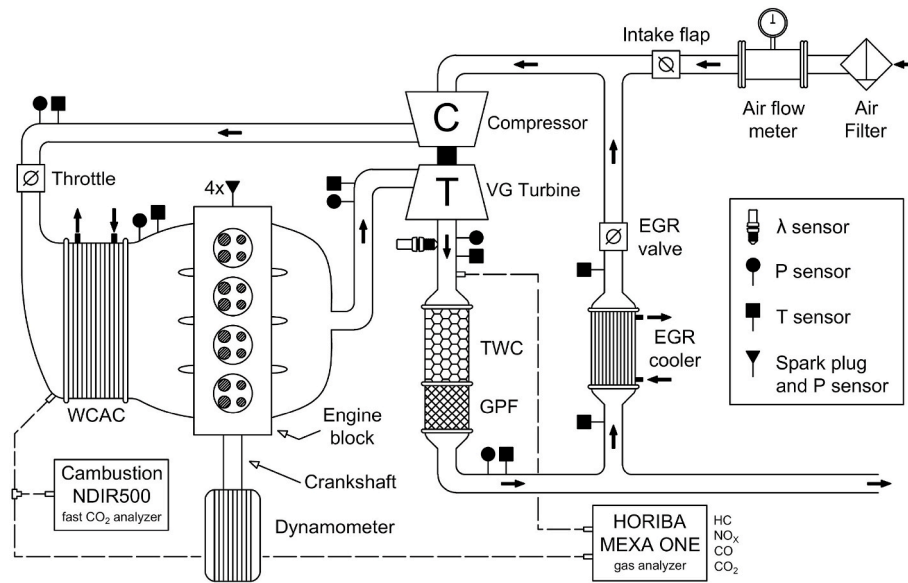


Fig. 1. Schematic engine's layout.

Crank-angle resolved pressure traces are measured in the four cylinders with pressure sensors integrated into the spark plugs (AVL Z133), and in the manifolds with Kitsler 601CAA piezoelectric type sensors. These pressure signals are registered with a frequency of 5 samples per CAD through the PXI 6123 and PXI 6251 acquisition modules, programmed with Labview by National Instruments TM [27]. The in-cylinder pressure traces are also processed to provide the real-time apparent heat release in the engine test rig, by which the combustion parameters are estimated [28]. Moreover, the engine control unit (ECU), designed for the original engine without EGR, is partially bypassed with the ETAS ES910 prototyping and interface module, enabling any modification of the VVT system, spark timing, injected fuel, and throttle position. The ECU is also equipped with an air flow meter, placed at the air-filter outlet, to guarantee a proper lambda control when operating with EGR. Finally, the PXI 7813R and NI 9759 control modules are used to manage the EGR valve, intake flap, and VGT position in open-loop configuration [27,28].

3. 1D engine model

A GT-Power 1D model of the entire SI gasoline engine described in Section 2 is used in this research, including the EGR, VVT, and VGT technologies. This model was already utilized in two previous studies [25,29] and calibrated according to the method defined in Ref. [30]. The model calibration consisted in applying empirical correlations to accurately reproduce engine phenomena, such as combustion process, heat transfer, and pressure drop. The procedure followed to obtain the said correlations is explained below. Firstly, around 300 engine tests distributed into 16 steady-state operating points were performed with varying EGR rates and VVT settings. Six EGR rates (0, 5, 10, 15, 20, and 25%) were tested per operating point for three valve overlap conditions (minimum, intermediate, and maximum). The spark timing was fixed in each test in real time, following the criterion that the optimal combustion start in SI engines generally leads to a value of CA50 (crank-angle degree at 50% heat release) between 5 and 10 CAD after top dead center [31]. The 16 working points mentioned above were selected to cover most of the engine operation during a WLTP driving cycle.

Those 300 experiments were then replicated with the 1D engine model to tune different fitting parameters, such as heat transfer multipliers, friction multipliers, and discharge coefficients. For that purpose, the 1D model was set in the following way: the turbocharger was decoupled by unlinking compressor and turbine powers to regulate the

intake and exhaust manifold pressures simultaneously; and besides, PI controllers were configured to modify the fitting parameters, in order to achieve the experimental cycle-averaged temperature and pressure values around the turbocharger and at the intake and exhaust manifolds. Later, a validation process was performed before obtaining the empirical correlations. The actual and predicted values of air mass flow (AMF) and indicated mean effective pressure (IMEP) were compared, and the instantaneous pressure traces in the cylinders and manifolds were checked. An error threshold of 5% was considered for both AMF and IMEP variables in the interest of reliability. In other words, the fitting parameters of each simulation were utilized as inputs for the correlations only if the corresponding AMF and IMEP relative errors were lower than 5%. The AMF and IMEP errors related to the 300 steady-state engine tests employed for the model calibration are respectively depicted in Fig. 2 and Fig. 3. In particular, three types of errors are provided for every operating point: mean percentage error (MPE), mean absolute percentage error (MAPE), and maximum error (in absolute value).

The MPE is a functional indicator to evaluate the calibration process, given that MPE values close to 0% mean that additional efforts to tune fitting parameters are useless. It should be noted that all AMF and IMEP maximum errors are inside the 5% threshold. After this validation, some empirical correlations were determined from the validated fitting parameters, and an artificial neural network (ANN) was trained with experimental and modeling data, as detailed in Ref. [30], to predict Wiebe function parameters for combustion simulation [32]. This way, the Wiebe parameters are sensitive to changes in operating conditions. Table 2 provides the following attributes of the correlations and ANN implemented into the model: (i) the involved variable; (ii) the fitting parameter or correlation output; (iii) the independent variables or inputs; (iv) the type of correlation; and (v) the coefficient of determination (R^2). The model calibration is completed with the implementation of these empirical correlations. Then, the turbocharger is recoupled, the PI controllers are removed, and the model is ready to be used in open-loop configuration. Besides, the 1D engine model includes hot-exposed turbocharger maps, which were formerly extrapolated and adiabaticized to enhance the limited data given by the manufacturers [33]. As adiabaticized maps are utilized, the heat transfer in the turbine volute is considered and adjusted by applying the same empirical correlation as for the exhaust manifold.

The pressurized air tank (PAT) and electric supercharger (e-supercharger) systems, proposed to improve the transient engine operation with EGR, are also added to the 1D engine model. Fig. 4 shows the GT-

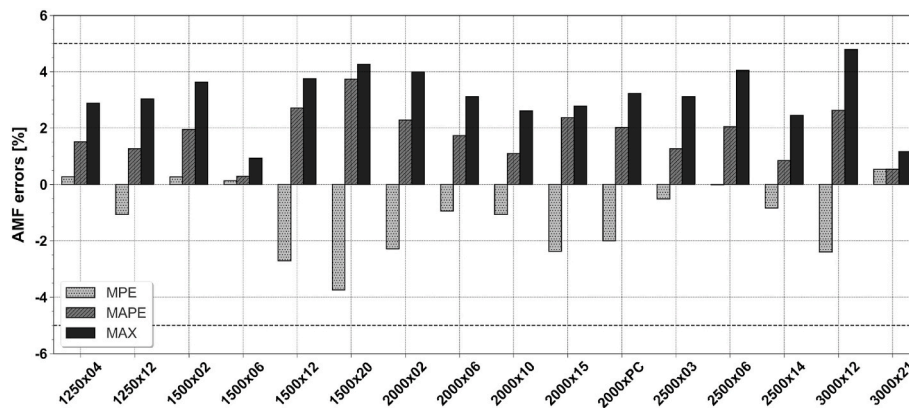


Fig. 2. Modeling AMF errors related to the 16 steady-state operating points selected for the model calibration [29]. In the x-axis labels, the first value is the engine speed (rpm), and the second is the engine BMEP (bar).

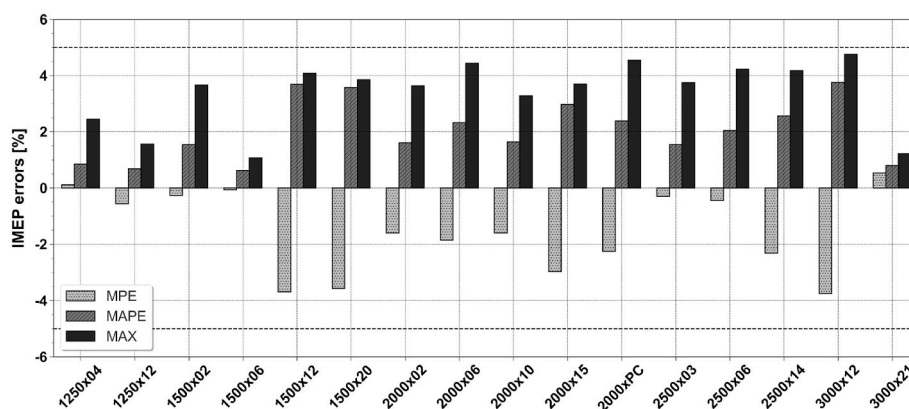


Fig. 3. Modeling IMEP errors related to the 16 steady-state operating points selected for the model calibration [29]. In the x-axis labels, the first value is the engine speed (rpm), and the second is the engine BMEP (bar).

Power schematic diagram of the complete intake path from the environment to the intake ports, including the low-pressure EGR, PAT and e-supercharger systems. The PAT sub-model is composed of a zero-dimensional air reservoir with a constant volume and a check valve (DN30). Two PAT configurations, named “upstream” and “downstream” due to the tank location regarding the compressor, are investigated. The downstream tank is directly connected to the intake manifold, while the upstream tank pressurizes the volume between the EGR joint and the compressor inlet. It should be stated that the intake flap and EGR valve are modeled in the upstream case as check valves to avoid reverse flow. The advantages and drawbacks of both configurations will be discussed later. Besides, the tank is equipped with an anti-vacuum valve to not operate below the ambient pressure. This scenario might happen with the upstream configuration when the intake flap is partially closed to achieve high EGR rates.

The electric supercharger is recreated with three elements: a basic electric motor (EM) that requires a single input, the output power; a shaft with a simple model of mechanical losses (1D lookup table with the shaft speed as the input variable) that also includes the losses in the electric motor; and a compressor fed with hot-exposed maps previously extrapolated and adiabaticized [33]. This system, along with a bypass valve, is installed downstream of the main compressor in series. In addition, a proportional controller is configured to regulate the EM output power based on the desired intake manifold pressure. The e-supercharger used in this paper is the same as the one researched in Ref. [34] and its main attributes are provided in Table 3.

4. Results and discussion

Tip-in maneuvers at 1500 rpm from 62 Nm (6 bar BMEP) to 124 Nm (12 bar BMEP) were tested and simulated to address the research objectives. It should be stated that the SI gasoline engine described in Section 2 operates with 21% and 23% EGR at the initial and final working points, respectively [25]. The tip-in tests are presented in two subsections: (4.1) EGR influence on transient engine response and (4.2) EGR reduction strategy. The tip-in simulation results are organized into three subsections: (4.3) validation of the transient 1D model performance, (4.4) pressurized air tank, and (4.5) electric supercharger. Finally, an overall analysis of all modeled and experimental data is provided in Section 4.6.

4.1. EGR influence on transient engine response

Two tip-ins were tested, one without EGR (labeled “target”) and the other with EGR (“baseline”), to analyze how high EGR operation affects the transient engine response. Fig. 5 shows the time evolution of the valve setpoints in both tip-in tests. The setpoints of the throttle, VGT, intake flap, VVT system, and spark timing were linearly changed from their initial to final values in two engine cycles. The EGR valve was kept fully open during the whole maneuver in the baseline case. All the actuators were synchronized using the pedal signal. Fig. 6 provides the time evolution of the intake manifold pressure (a), air mass flow (b), turbocharger speed (c), and torque (d) in the target and baseline tip-ins. A significantly slower air mass flow increase is observed in the case with EGR, resulting in poor engine response. This behavior is due to the need

Table 2

Attributes of the empirical correlations and ANN implemented into the 1D engine model [29]. (*) R² related to the ANN training data set.

Involved variable	Fitting parameter	Independent variables	Correlation type	R ²
Intake manifold pressure	Throttle discharge coefficient	Throttle angle	Look-up table	–
Intake manifold temperature	WCAC	Engine speed and IMEP	3D map from scattered data	–
Turbine inlet temperature	Heat transfer multiplier of exhaust manifold	Exhaust ports temperature and exhaust gases mass flow	Linear polynomial equation	0.81
Aftertreatment pressure drop	FWC pressure drop	FWC gas volume flow	Look-up table	–
Exhaust line pressure drop	Exhaust line pressure drop	Exhaust line gas volume flow	Look-up table	–
EGR cooler inlet temperature	Heat transfer multiplier of EGR line	FWC outlet temperature and EGR flow	Linear polynomial equation	0.75
EGR cooler outlet temperature	Coolant flow in the EGR cooler	Engine speed and IMEP	3D map from scattered data	–
Combustion phasing (Wiebe function)	CA50	Spark timing, AFR, engine speed and in-cylinder pressure, temperature, trapped mass and residual gas fraction at IVC.	Quadratic polynomial neural network	0.98*
Combustion duration (Wiebe function)	CA1090	Spark timing, AFR, engine speed and in-cylinder pressure, temperature, trapped mass and residual gas fraction at IVC.	Quadratic polynomial neural network	0.96*
Engine friction losses	FMEP	Engine speed and maximum cylinder pressure	Chen-Flynn model	0.81

for higher turbocharger acceleration, given that introducing 23% of EGR requires an additional pressure increment of around 0.20 bar in the intake manifold to achieve the final torque (124 Nm). Comparing the torque evolution in both tip-ins reveals that the EGR strategy leads to a 2-s slower response time (Fig. 6d). The response time is defined in this research as the time required to complete the 95% of the total load increase; in other words, the time spent to reach a torque value of 120 Nm.

4.2. EGR reduction strategy

Given the poor engine response with EGR, reducing the EGR dilution during the first engine cycles of the tip-in was proposed as a strategy to accelerate the torque increase. This strategy basically consists in modifying the EGR valve actuation as follows: instead of keeping the EGR valve fully open as in the baseline tip-in, it is closed as fast as possible simultaneously with the throttle opening, kept closed for some engine cycles, and finally, reopened slowly. A total of twenty tip-in maneuvers divided into two stages were tested to determine the duration of the EGR valve closure and the slope of the reopening ramp. Ten tip-in tests were performed in the first stage with varying durations (3, 5, 7, 9, and 11 cycles) and slopes (40 and 80 units of opening per second). A conservative spark timing was used in this stage to prevent knocking. The same ten tip-ins were repeated in the second stage, but now adjusting the spark timing actuation based on the fast intake CO₂ measurements to improve combustion. The best of these ten tip-ins in terms of torque response (labeled “Case A”) is the one that combines an EGR valve

closure of 7 cycles with a reopening slope of 40.

Fig. 7 provides the time evolution of the EGR valve (a) and spark timing (b) setpoints in the “baseline” and “Case A” tip-in tests. The rest of the valve actuations in Case A are the same as in the baseline (Fig. 5). Fig. 8 shows the time evolution of the intake manifold pressure (a), air mass flow (b), turbine inlet temperature (c), intake manifold CO₂ volume fraction (d), torque (e), and turbocharger speed (f) in the “baseline” and “Case A” tip-in tests. Closing the EGR valve at the maneuver beginning improves torque response significantly, mainly due to a sharp increase in AMF before 0.4 s. Besides, higher enthalpy is provided to the turbine in Case A, resulting in a better turbocharger acceleration (Fig. 8f). The response time in Case A is around 0.57 s, only 0.25 s slower than in the target case without EGR and 1.75 s faster than in the baseline case. Finally, it should be remarked that the torque overshoot observed after 0.8 s (Fig. 8e) can be avoided by adjusting the EGR valve actuation, as will be shown in Section 4.6.

4.3. Engine model validation

Although the EGR reduction strategy substantially shortens the torque response time, there is room for further improvement. To this end, the PAT and e-supercharger systems are investigated utilizing the 1D engine model (Section 3). Before that, the “Case A” tip-in test was simulated to validate the model performance under transient conditions. The procedure followed to reproduce the said tip-in is described below. The experimental throttle, EGR valve, and intake flap actuations were directly imposed into the model, and the VGT position was adjusted during the simulation to follow the pressure evolution in the intake manifold. This adjustment is fully explained in Ref. [35] and mainly consists in applying a slight correction to the VGT position measurement using a PI controller. The experimental values of the spark timing, air-to-fuel ratio, and VVT system settings were also given to the model as inputs. Besides, some thermocouples were modeled to consider the thermal inertia of actual sensors in the most relevant engine parts, such as turbine inlet and outlet, compressor outlet, and intake manifold. Regarding the combustion, the Wiebe function parameters were predicted through the ANN. Fig. 9 shows the time evolution of the following experimental and modeled variables in the “Case A” tip-in: intake and exhaust manifold pressures (a), air mass flow (b), turbocharger speed (c), intake CO₂ volume fraction (d), indicated and brake mean effective pressures (e), and turbine inlet temperature (f).

The model prediction is quite accurate in general terms. The pressure evolution in the intake manifold is perfectly reproduced by tuning the VGT position (errors lower than 1%). The exhaust manifold pressure is also well replicated, but differences of up to 4% are detected at around 0.8 s. Such differences are probably due to a slight overprediction of the turbine efficiency. In addition, no noticeable errors in the intake CO₂ fraction and AMF variables are observed, so the 1D model reproduces the air management process with high accuracy. If the intake flow and composition are achieved, the precise modeling of the IMEP and BMEP demonstrates that the Wiebe parameters (ANN) and FMEP (Chen-Flynn model) are well predicted. After 1.2 s, the model does not capture some torque fluctuations induced by combustion instabilities or cycle-to-cycle dispersion, given that these phenomena were not considered for the ANN training. The turbine inlet temperature is replicated with errors lower than 5° Celsius (°C), so the performance of the heat transfer correlation applied to the exhaust manifold is remarkable. Finally, the accurate modeling of the turbocharger speed corroborates the high accuracy of the turbine and compressor maps.

4.4. Pressurized air tank (PAT)

A 2-L tank of fresh air, initially at 20 °C and 3 bar, was used for all simulations presented in this section. It was assumed that larger tank volumes would not be viable because of space restrictions. The initial tank pressure was selected to obtain the same torque response time as in

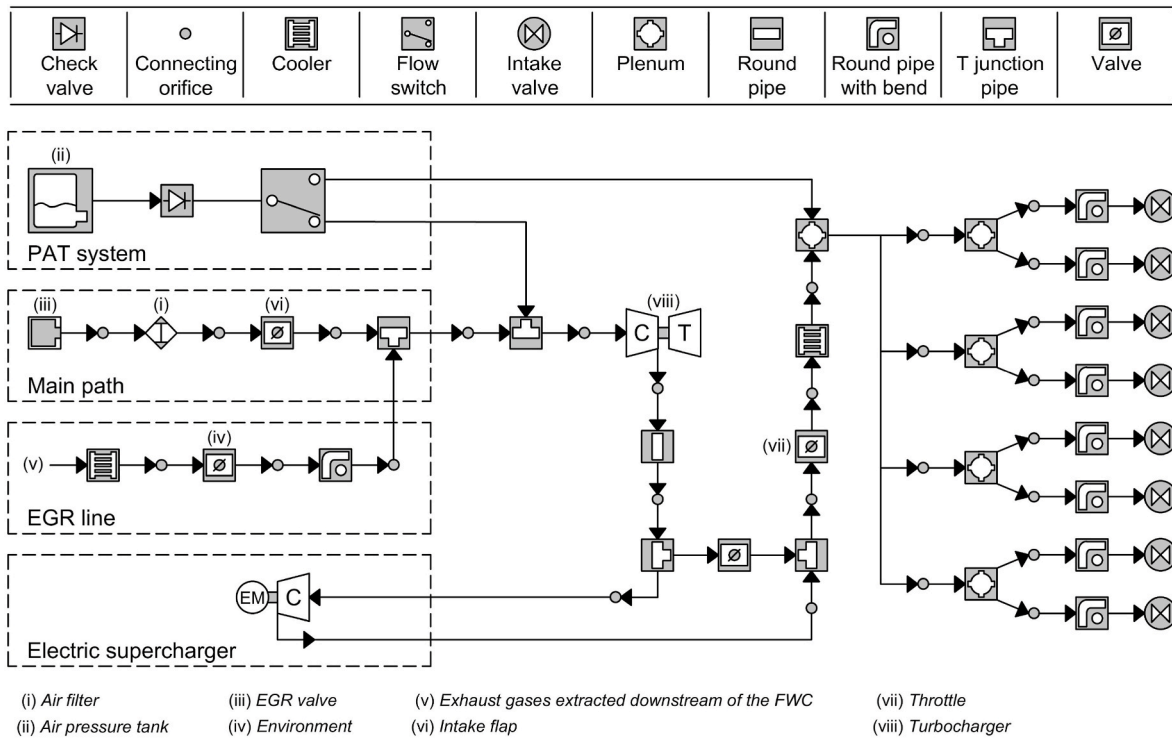


Fig. 4. GT-Power schematic diagram of the whole engine intake path, including the EGR, PAT and electric supercharger systems.

Table 3
Electric supercharger's attributes.

Attribute	Description
Inertia	$2.4 \cdot 10^{-6} \text{ kg m}^2$
Maximum compression ratio	1.5
Maximum compressor efficiency	0.85
Maximum electrical power	2000 W
Maximum speed	70,000 rpm

the “target” tip-in without EGR. After trying different values, it was found that an initial tank pressure of at least 3 bar is required. Tip-in simulation results with other initial tank pressure values were omitted for brevity. Two PAT configurations or locations were studied: downstream and upstream. The downstream tank is directly connected to the intake manifold to increase the in-cylinder trapped air mass quickly. However, this configuration leads to the compressor blocking (surge)

and requires a transient EGR valve closure, as in Case A, to avoid the torque drop once the tank empties. Alternatively, the upstream PAT is linked to the volume between the EGR junction and the compressor inlet (Fig. 4). In this way, the tank does not block the compressor, although its implementation involves using check valves to prevent reverse flow through the EGR valve and intake flap. Both downstream and upstream PAT strategies are explained in detail below. Finally, it should be remarked that the tank filling procedure is not addressed in this research.

4.4.1. Downstream PAT

Given that the amount of pressurized air is limited (only 2 L), the opening timing of the tank valve is critical to achieving good results. Six tip-ins were first simulated with the downstream PAT, applying three delays to the tank valve opening (0, 2, and 4 engine cycles regarding the throttle opening) for two different EGR valve actuations (fully open and

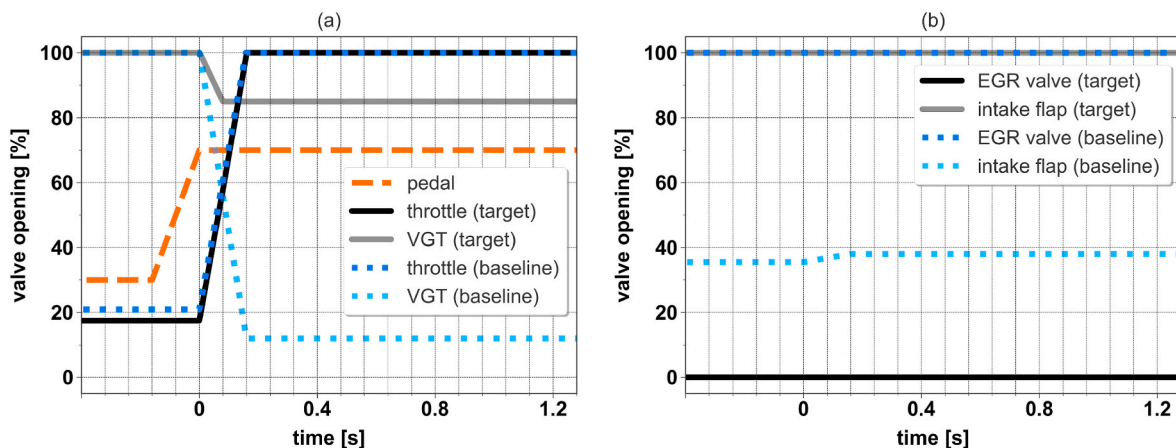


Fig. 5. Time evolution of the throttle and VGT setpoints (a) and EGR valve and intake flap setpoints (b) in the target (case without EGR) and baseline (with EGR) tip-in tests.

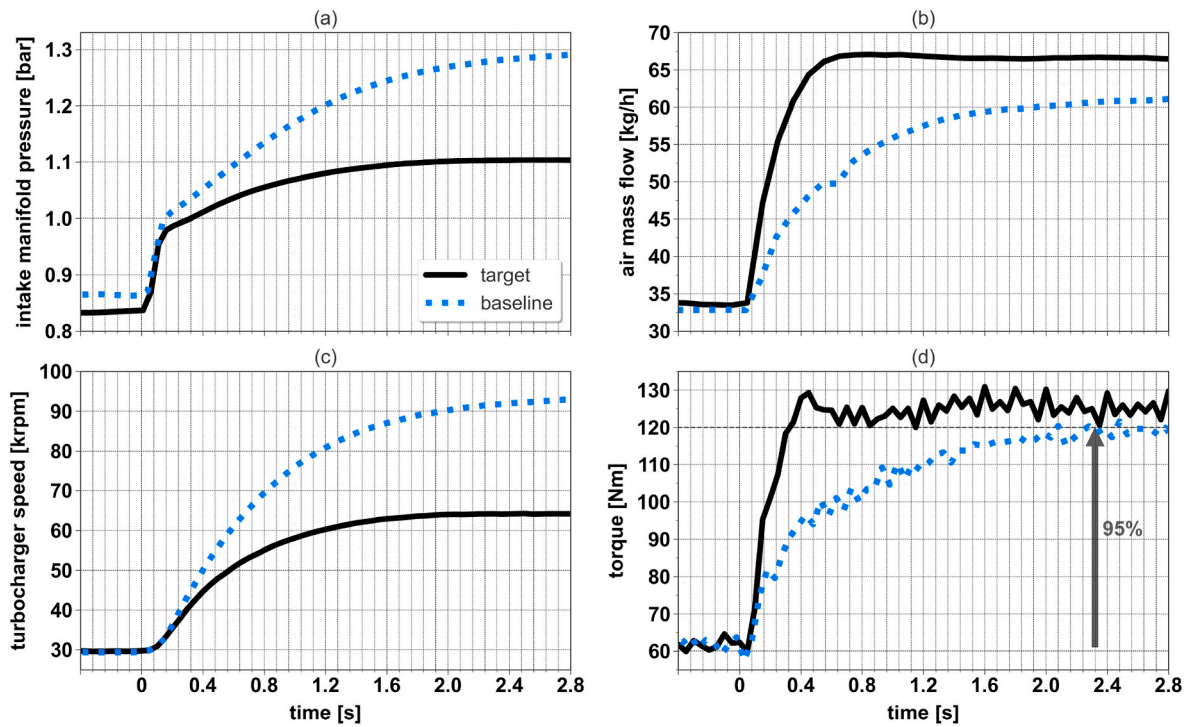


Fig. 6. Time evolution of the intake manifold pressure (a), air mass flow (b), turbocharger speed (c), and torque (d) in the target (without EGR) and baseline (with EGR) tip-in tests.

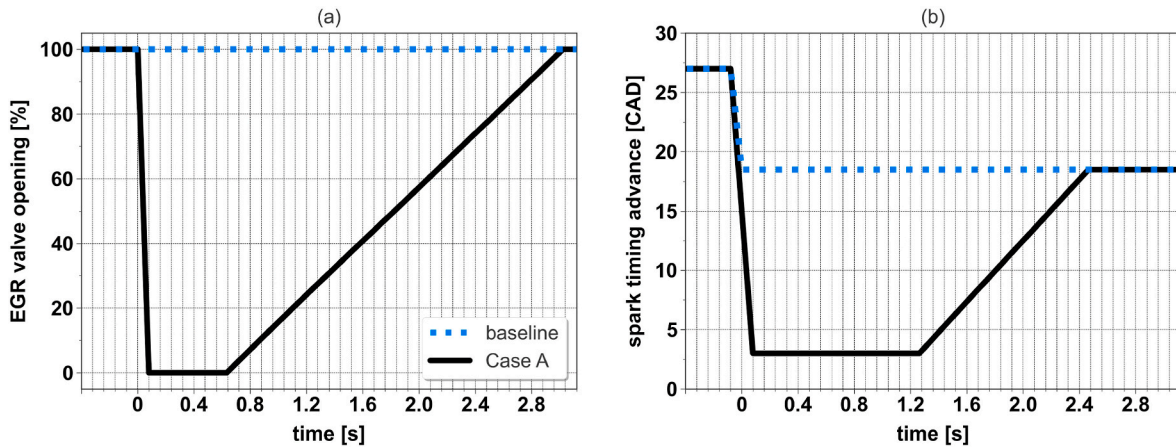


Fig. 7. Time evolution of the EGR valve (a) and spark timing (b) setpoints in the “baseline” and “Case A” tip-in tests.

partially closed). Fig. 10 provides the positions of the EGR and tank valves during these six tip-in simulations. The rest of the valve actuations are the same as those used to reproduce the “Case A” tip-in (Section 4.3). Besides, the stoichiometric air-to-fuel ratio is imposed throughout the maneuver, and the Wiebe function parameters are predicted using the ANN. Fig. 11 shows the time evolution of the AMF through the PAT valve (a) and intake ports (b), EGR rate at the intake ports (c), and engine torque (d) in the six tip-in simulations.

The best engine torque response is achieved by delaying the PAT valve opening by two cycles and closing the EGR valve partially at the maneuver beginning (as in Case A). The response time is not reduced when opening the PAT valve simultaneously with the throttle due to the short-circuit of a portion of the pressurized air. As seen in Fig. 11, the peak of AMF (through the intake ports) at 0.15 s does not result in a proportional torque increase. Although this short-circuit phenomenon occurs in the six cases, it is more significant when the tank valve opening

is not delayed. This is because the abrupt pressure increase in the intake manifold takes place while the valve overlap is still quite long. It should be stated that the VVT system is configured to provide a valve overlap of around 60 and 15 CAD at the initial and final tip-in operating conditions, respectively. The transition between the initial and final VVT settings lasts three cycles. Regarding the EGR valve actuation, it should be noted that reducing the EGR dilution in the first 2 s is mandatory to avoid a torque drop once the tank becomes empty.

As a drawback, the downstream PAT strategy leads to compressor surge, given that the intake path is blocked. Surge appearance can be prevented, as in tip-out maneuvers [36,37], using a recirculation (or anti-surge) valve that connects the inlet and outlet of the compressor when it approaches the surge limit. This recirculation valve was inserted into the 1D engine model, and the tip-in with the best torque response time of the six cases in Fig. 11 was re-simulated. The anti-surge valve was opened in this simulation when the compressor operating point

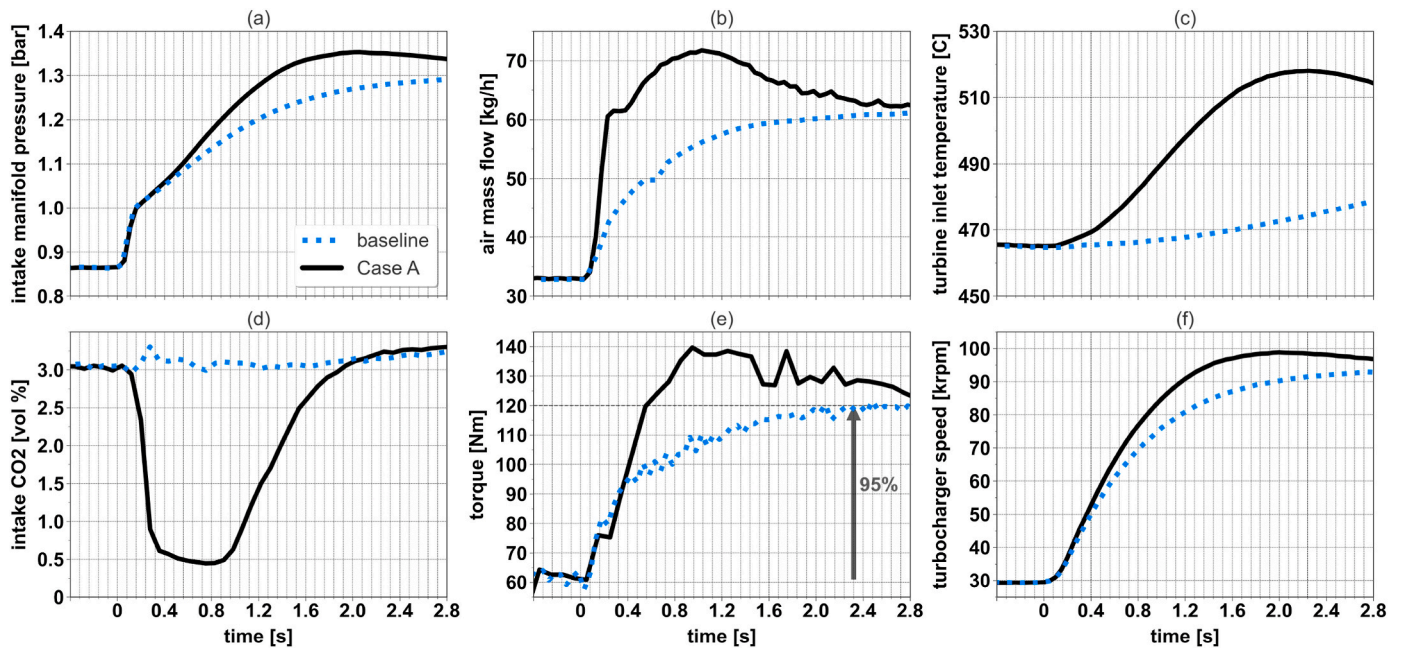


Fig. 8. Time evolution of the intake manifold pressure (a), air mass flow (b), turbine inlet temperature (c), intake CO₂ volume fraction (d), torque (e), and turbocharger speed (f) in the “baseline” and “Case A” tip-in tests.

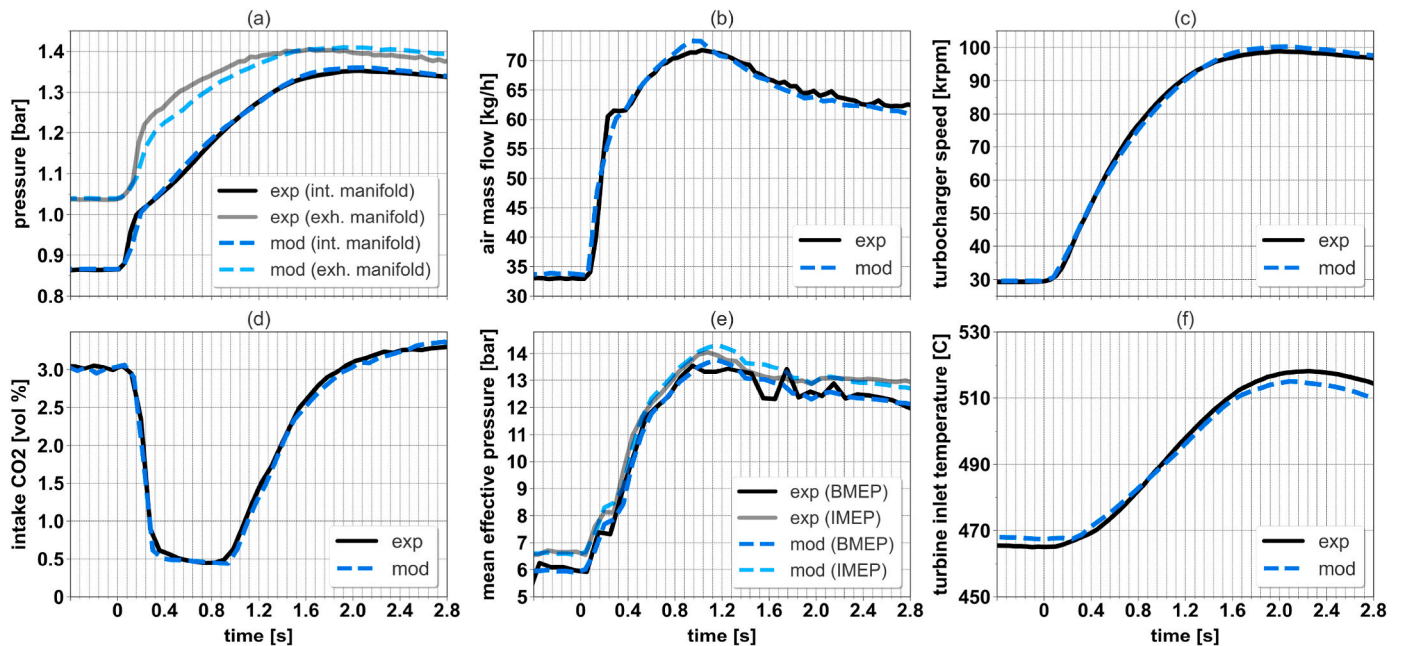


Fig. 9. Time evolution of the following actual (exp) and predicted (mod) variables in the “Case A” tip-in: intake and exhaust manifold pressures (a), air mass flow (b), turbocharger speed (c), intake CO₂ volume fraction (d), indicated and brake mean effective pressures (e), and turbine inlet temperature (f).

exceeded the surge line, which was experimentally measured under steady-state non-pulsating flow conditions. Fig. 12 depicts the compressor operating path (a), engine torque (b), AMF through the throttle and intake ports (c), and EGR rate at the intake ports (d) during two tip-in simulations: the case with a 2-cycle delay in the PAT valve opening and with a transient EGR valve closure, presented in Fig. 11 (solid black line), and the same case but with compressor surge mitigation (dotted blue line). The flow recirculation through the anti-surge valve results in a negative mass flow rate in the throttle, slightly penalizing the engine torque increase. This was compensated by further reducing the EGR valve opening, as noticed in the time evolution of the

EGR rate at the intake ports in the case with no surge in Fig. 12d. After these simulations, it is concluded that a 0.31-s torque response time is achieved by combining the downstream PAT and EGR reduction strategies.

4.4.2. Upstream PAT

A series of tip-in simulations were performed with the upstream tank to optimize the PAT valve opening. Because of the larger distance between the tank and cylinders, the best engine torque response is obtained by opening the PAT valve simultaneously with the throttle. Besides, it should be remarked that closing the EGR valve is not required

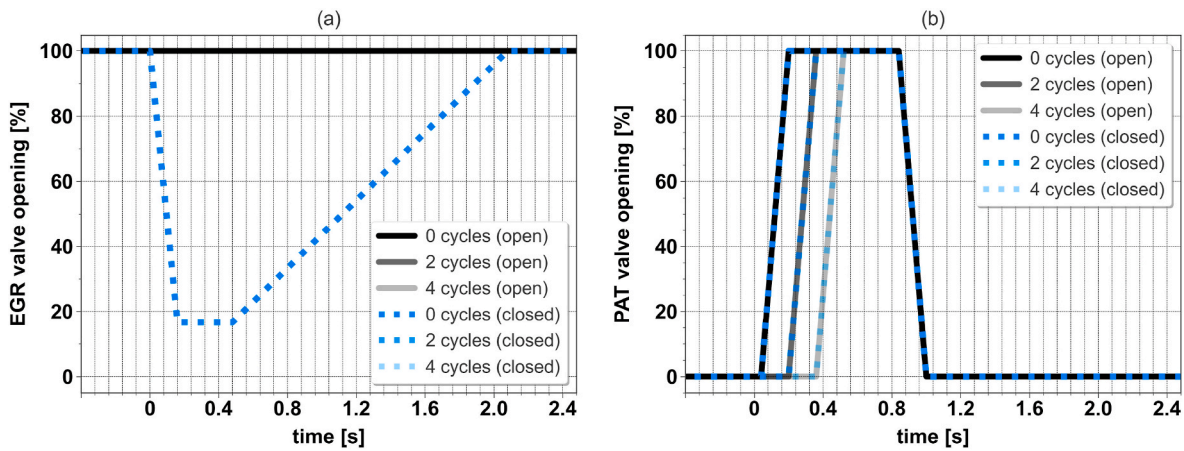


Fig. 10. EGR (a) and PAT (b) valves' actuations in the six tip-in simulations with the downstream PAT. In the legend, the first term shows the PAT valve opening delay in cycles (regarding the throttle opening), and the second (in parentheses) is related to the EGR valve position.

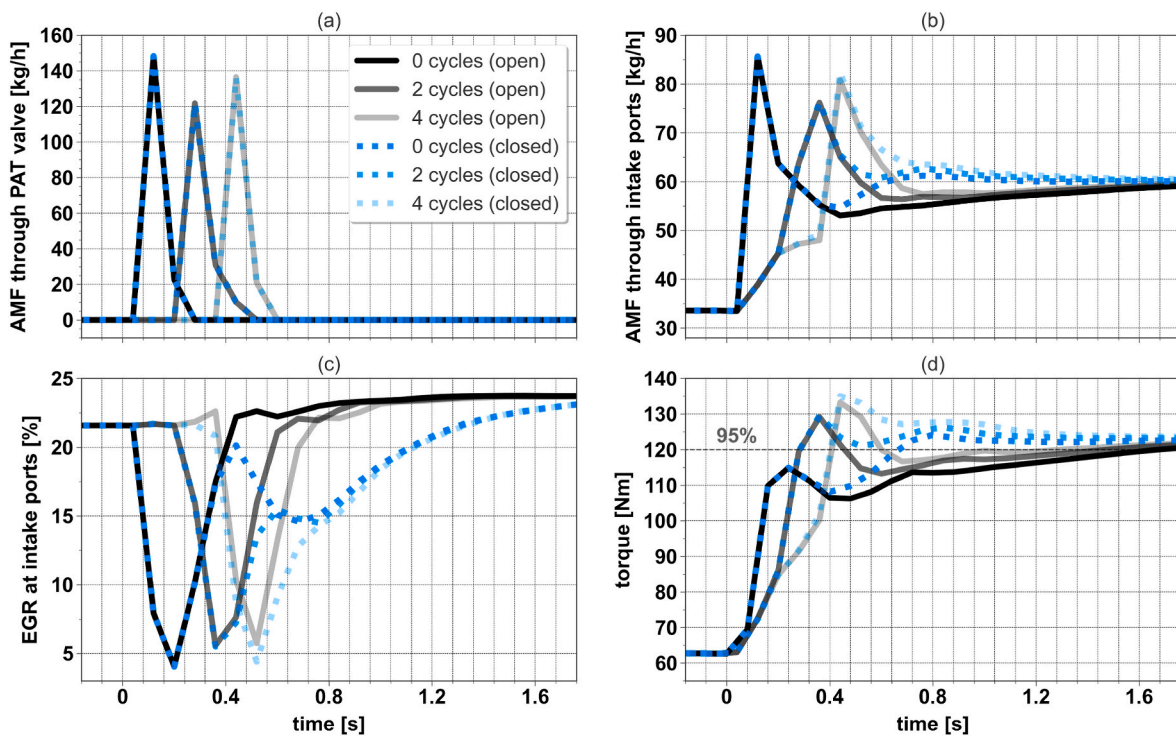


Fig. 11. Time evolution of the AMF through the PAT valve (a) and intake ports (b), EGR rate at the intake ports (c), and torque (d) in the six tip-in simulations with the downstream PAT. In the legend, the first term shows the PAT valve opening delay in cycles (regarding the throttle opening), and the second (in parentheses) is related to the EGR valve position.

to prevent the torque drop after the tank emptying. The EGR dilution can be reduced using the PAT even when depressurized, given that it is connected to the compressor inlet where the pressure is slightly lower than the ambient. It should be reminded that the tank is equipped with an anti-vacuum valve (Section 3). Fig. 13 provides the time evolution of the AMF through the PAT valve (a) and intake ports (b), EGR rate at the intake ports (c), and engine torque (d) in the two following tip-in simulations: the best case with the downstream PAT without surge (labeled “Case B”), previously presented in Fig. 12; and the best solution with the upstream PAT (“Case C”) by opening the tank valve with no delay and keeping the EGR valve open. In both simulations, the Wiebe function parameters were predicted using the ANN, and the stoichiometric air-to-fuel ratio was imposed throughout the tip-in.

As observed in Fig. 13, the tank valve opening in Case C is extended

until the turbocharger provides the desired boost pressure, thus sustaining the EGR dilution below 20% in the first 1.3 s. Regarding the torque, the response time in Case C is around 0.43 s, 0.12 s slower than in Case B with the downstream tank.

4.5. Electric supercharger

One tip-in simulation was carried out with the electric supercharger (e-supercharger), which was actuated simultaneously with the throttle opening. The output power of the electric motor was regulated using a proportional controller to reach and maintain the intake manifold pressure target (1.3 bar). The peak power consumed by the e-supercharger was around 90% of its maximum capacity. The rest of the valve actuations were the same as in the baseline tip-in; that is, the valve

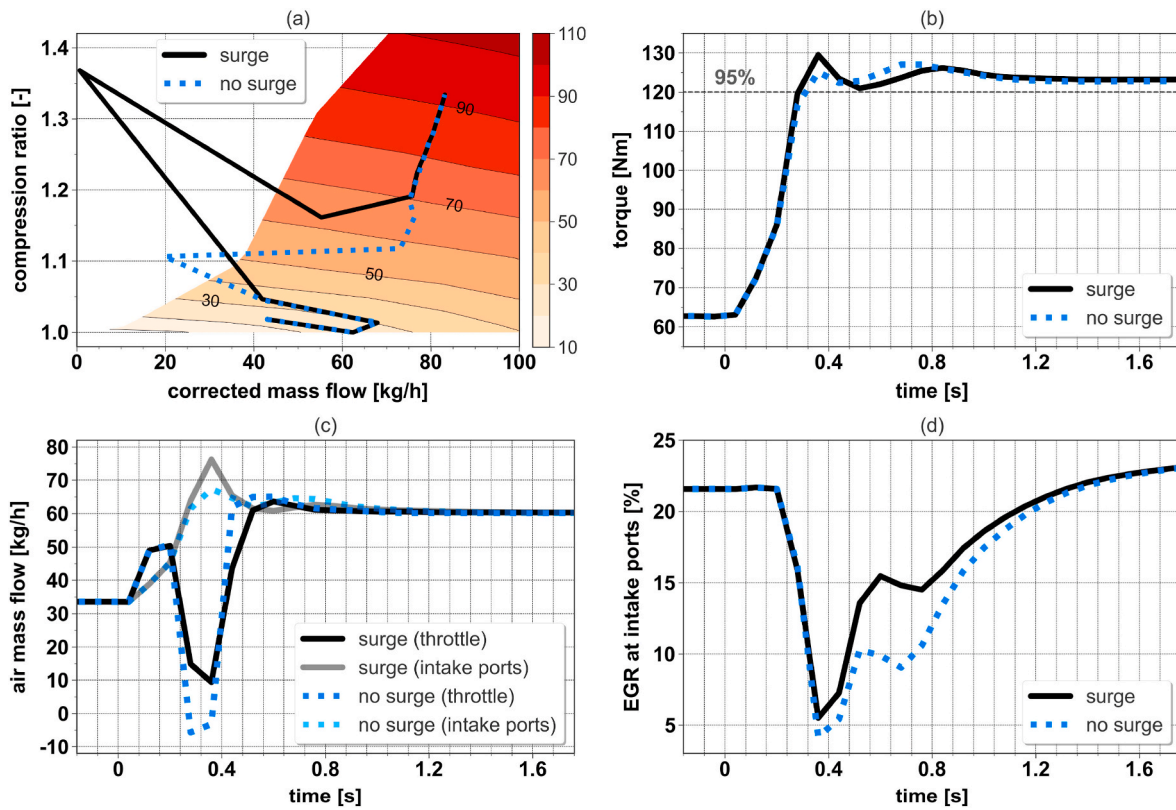


Fig. 12. Compressor operating path (a), engine torque (b), AMF through the throttle and intake ports (c), and EGR rate at the intake ports (d) during the best tip-in simulation applying the downstream PAT strategy with (dotted blue line) and without (solid black line) compressor surge mitigation. The corrected compressor speed values are given in the vertical colorbar in kRPM.

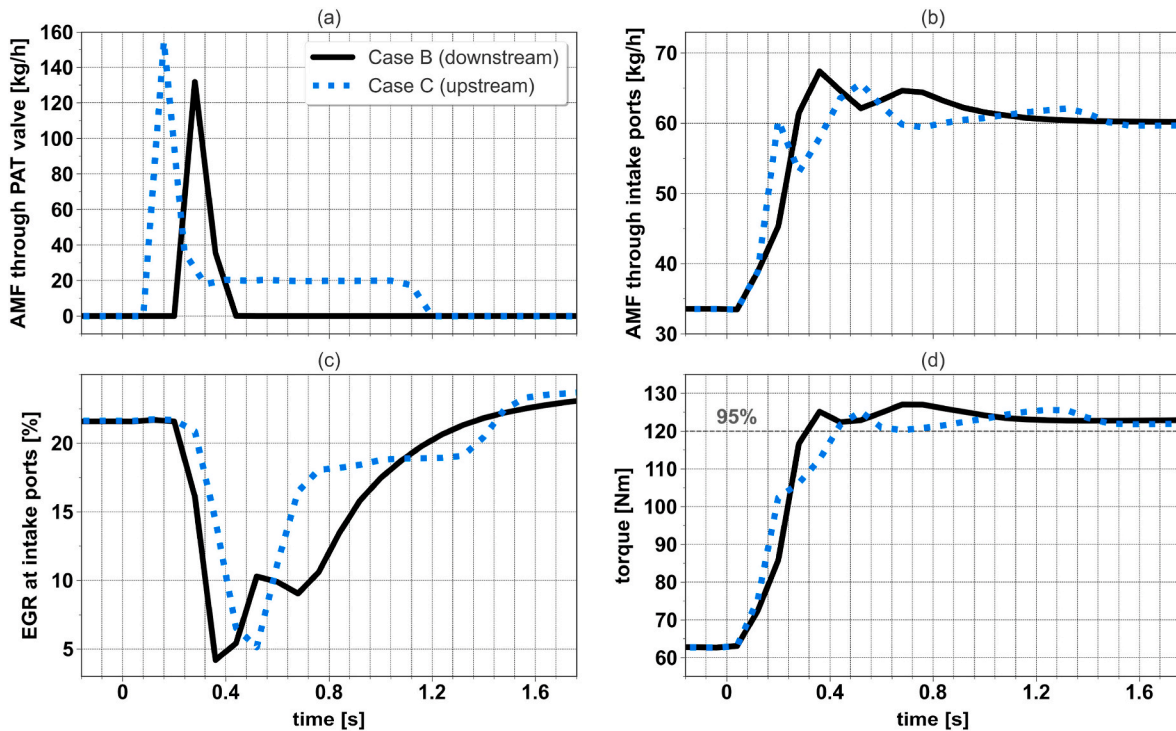


Fig. 13. Time evolution of the AMF through the PAT valve (a) and intake ports (b), EGR rate at the intake ports (c), and engine torque (d) in the “Case B” and “Case C” tip-in simulations.

positions were linearly changed in two engine cycles, and the EGR valve was kept open throughout the simulation. Besides, the ANN was utilized to estimate the Wiebe function parameters, and a constant air-to-fuel ratio equal to the stoichiometric was imposed. Fig. 14 shows the e-supercharger operating path (a) and speed (b), intake manifold pressure (c), and engine torque (d) during the tip-in simulation with the electric supercharger (labeled “Case D”). The supercharger reaches 48.000 rpm in 0.25 s, providing a maximum pressure ratio of 1.2. This leads to a fast pressure increase in the intake manifold without the need to reduce the EGR dilution. Regarding the engine torque, it can be concluded that the electric supercharger reduces the response time to 0.41 s.

4.6. Overall analysis

This section comprehensively compares the four air management solutions, mainly based on the torque response and fuel economy. Besides, other criteria, such as complexity and material costs, are also considered. To guarantee a fair comparison, the EGR valve actuation in Case A was adjusted via modeling to avoid the torque overshoot seen in Fig. 8e. The torque overshoot was eliminated by combining an EGR valve closure of 4 engine cycles (instead of 7) with a reopening slope of 35 units per second (instead of 40). The tip-in simulation with the adjusted EGR valve actuation was labeled “Case A+”. For the sake of readability, Table 4 shows the main characteristics of the four solutions studied: EGR reduction (Case A+), downstream PAT with EGR reduction (Case B), upstream PAT (Case C), and electric supercharger (Case D).

Fig. 15 provides the predicted time evolution of the AMF through the intake ports (a), EGR rate at intake ports (b), engine torque (c), and corrected BSFC (d) in Cases A+, B, C, and D. The time evolution of the engine torque in the “target” and “baseline” tip-in tests is also depicted in Fig. 15. The corrected BSFC (brake specific fuel consumption) includes a fuel penalty to consider the power supplied by the auxiliary boosting system (\dot{W}_{sys}) and is calculated through Eq. (2):

Table 4
Main characteristics of the four air management solutions: Case A+, B, C, and D. (+) The EGR valve actuation in Case A was corrected to avoid torque overshoot.

Case	Strategy	EGR valve	Description EMS
A+	EGR reduction	Closed	The EGR dilution is transiently reduced. The EGR valve is closed quickly, kept closed for 4 cycles, and reopened slowly in 35 cycles.
B	Downstream PAT with EGR reduction	Partially closed	A 2-L air tank at 3 bar is connected to the intake manifold, and the tank valve is opened in 2 cycles after the throttle opening. The EGR valve is closed until the 17% opening, kept in this position for 4 cycles, and reopened in 20 cycles. The compressor anti-surge valve is opened for a very short time.
C	Upstream PAT	Open	A 2-L air tank at 3 bar is connected to the compressor inlet volume, and the tank valve is opened with no delay.
D	Electric supercharger	Open	An electric supercharger is installed downstream of the compressor in series and actuated with no delay.

$$BSFC^*(i) = \frac{\dot{m}_f(i) + \overline{BSFC} \cdot \dot{W}_{sys}(i)}{\dot{W}_{eng}(i)} \quad (2)$$

where $BSFC^*(i)$ is the corrected BSFC in the engine cycle i , \dot{m}_f the fuel mass flow rate (g/h), and \dot{W}_{eng} the engine power (kW). The constant term \overline{BSFC} refers to the averaged BSFC (290 g/kWh) of the SI engine used in this research working in a 1500-kg sport utility vehicle during a WLTP homologation cycle [29]. The power supplied by the auxiliary boosting system sys is calculated as follows:

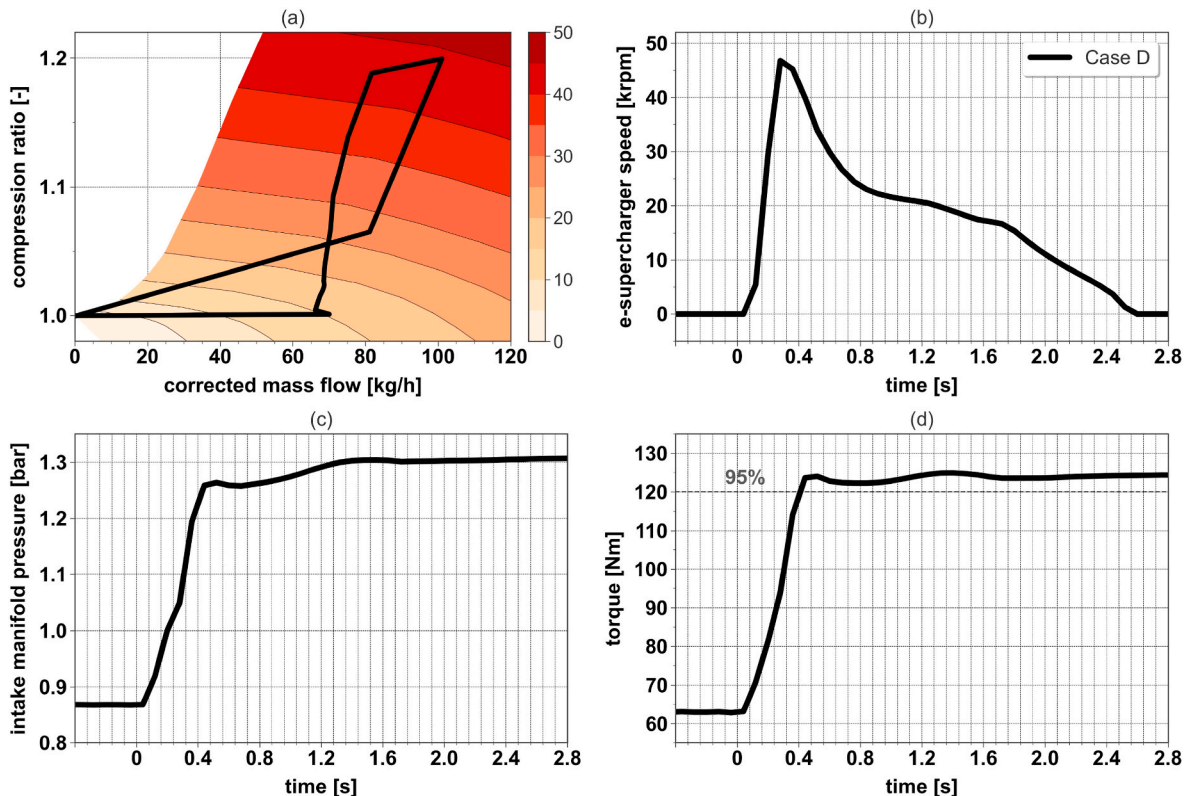


Fig. 14. Electric supercharger operating path (a) and speed (b), intake manifold pressure (c), and engine torque (d) during the “Case D” tip-in simulation.

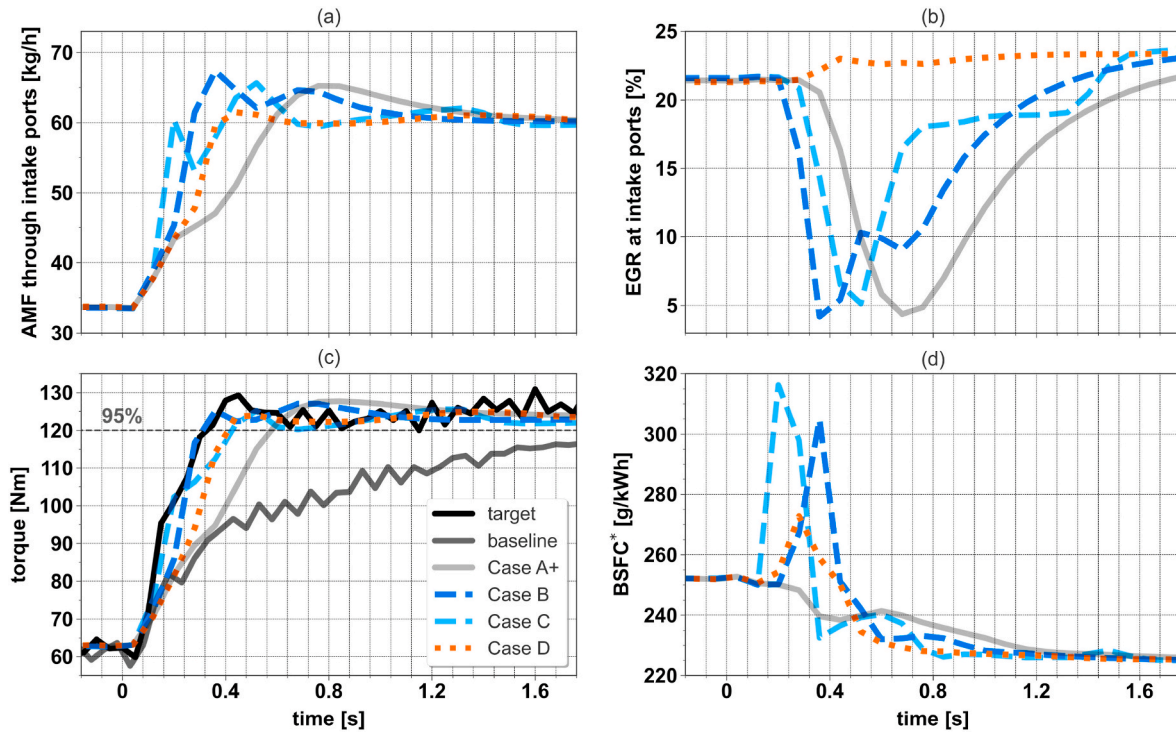


Fig. 15. Predicted time evolution of the AMF through the intake ports (a), EGR rate at intake ports (b), engine torque (c), and corrected BSFC (d) in Cases A+, B, C, and D. The torque evolution in the “target” and “baseline” tip-in tests is also included.

$$\dot{W}_{sys}(i) = \begin{cases} V_{tank} \frac{p_{tank}(i-1) - p_{tank}(i)}{T}, & \text{if } sys \text{ is the tank} \\ \dot{W}_{e-s}(i), & \text{if } sys \text{ is the electric supercharger} \end{cases} \quad (3)$$

where V_{tank} is the tank volume, p_{tank} the tank pressure, and T the duration of one engine cycle (0.08 s). The term $\dot{W}_{e-s}(i)$ is the output power of the supercharger electric motor.

Fig. 16 provides the average of the corrected BSFC (averaged $BSFC^*$) in the first 20 cycles (1.6 s) versus the torque response time for Cases A+, B, C, and D. A period of 20 cycles is selected for the averaged $BSFC^*$ because, after that time, the engine operating conditions (speed, load, and EGR) are practically stable in the four cases (Fig. 15). The averaged $BSFC^*$ is calculated as shown in Eq. (4):

$$averaged\ BSFC^* = \frac{\sum_{i=1}^{20} \dot{m}_f(i) + \overline{BSFC} \cdot \dot{W}_{sys}(i)}{\sum_{i=1}^{20} \dot{W}_{eng}(i)} \quad (4)$$

The EGR reduction strategy (Case A+) is the simplest and provides an acceptable torque response time (0.57 s) without any additional equipment. Having said that, implementing this strategy is not easy, given that the EGR valve and spark plug actuations must be adapted according to the operating conditions of each tip-in maneuver to avoid knocking and torque overshoot. The shortest response time (0.31 s) is achieved with the downstream PAT (Case B), even being slightly better than in the target tip-in without EGR (Fig. 15c). Nevertheless, applying the downstream PAT strategy involves a higher fuel consumption (Fig. 16), an added material expense, and a notable increase in complexity:

- Depending on the tip-in operating conditions, different initial tank pressure values may be needed.
- A tank filling procedure must be defined.
- Unless the tank volume or pressure is increased, reducing the EGR dilution is required to avoid the torque drop once the tank becomes empty. Consequently, the spark timing must be adjusted too.
- The PAT valve actuation is also critical unless the tank size is enlarged.
- Surge appearance must be mitigated since the downstream PAT blocks the compressor.

The upstream PAT solution (Case C) is a bit simpler, given that the EGR valve closure is not needed and that the compressor does not go into surge during the maneuver. It must be reminded that the EGR dilution in Case C is decreased using the tank itself due to its location. By contrast, the torque response time with the upstream PAT (0.43 s) is not as fast as with the downstream tank (Fig. 15c). Besides, installing the tank upstream of the compressor requires the employ of check valves to prevent

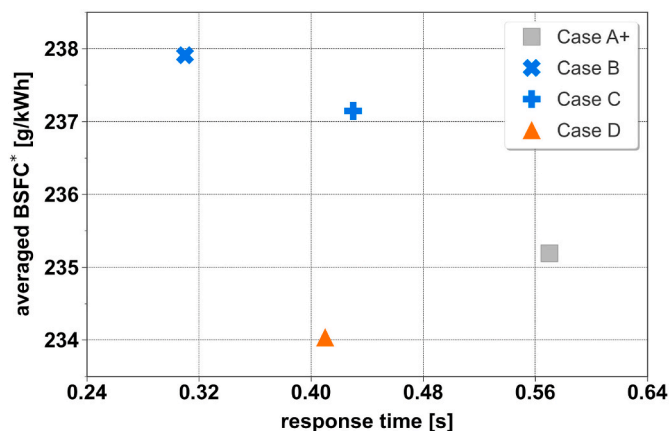


Fig. 16. Corrected BSFC average in the first 20 cycles (1.6 s) versus the torque response time for Cases A+, B, C, and D.

reverse flow through the EGR valve and intake flap.

By using the electric supercharger, a torque response time of 0.41 s is achieved while maintaining the EGR dilution above 21% (Fig. 15b). Operating with high EGR levels throughout the tip-in makes a difference in fuel consumption, causing the BSFC in Case D to be 1.6% lower than in Case B if considering the first 20 cycles (Fig. 16). Regarding the BSFC evolution in Fig. 15d, it should be stated that the peaks noticed in Cases B, C, and D before 0.4 s are because of the short-circuit of a part of the intake gases and, mainly, the fuel penalty related to the added boosting systems. Finally, it should also be remarked that utilizing the e-supercharger does not entail a significant increase in complexity. It only requires the management of the electric motor to obtain the desired boost pressure.

5. Summary and conclusions

The research objectives are to analyze the impact of high EGR operation on the transient response of a SI gasoline engine and assess the potential of three air management strategies to improve this response. Such strategies are: reducing EGR dilution by closing the EGR valve quickly at the maneuver beginning; using a pressurized air tank linked to the intake manifold (downstream PAT) or to the compressor inlet (upstream PAT); and connecting an electric supercharger to the compressor outlet in series. To address the objectives, tip-in maneuvers at 1500 rpm from 62 Nm (6 bar BMEP) to 124 Nm (12 bar BMEP) were tested and simulated. A 1D engine model, already validated for a wide range of steady-state operating conditions in previous studies, was used to perform tip-in simulations. Besides, in the reliability interest, the 1D model was validated under transient conditions utilizing the information from the tip-in tests.

Firstly, two tip-in tests were carried out to analyze the EGR effect on the engine torque response: one without EGR (target) and the other with EGR (baseline). In the baseline case, the gasoline engine operates with EGR rates higher than 21%. These experiments revealed that high EGR operation results in a 2-s slower torque response time (considering the time spent to complete the 95% of the total load increase). Then, the EGR reduction strategy was proposed to accelerate the load increase. This strategy mainly consists in closing the EGR valve as fast as possible, simultaneously with the throttle opening, and reopening it slowly after some engine cycles. A series of tip-in tests and simulations were performed to find the optimum EGR valve actuation. The EGR reduction strategy substantially improves the engine response without any additional equipment, leading to a response time of 0.57 s, only 0.25 s slower than in the target case without EGR.

The PAT and e-supercharger strategies were exclusively investigated via 1D modeling. A 2-L air tank, initially at 3 bar, was added to the engine model to evaluate the two PAT solutions. In both cases, some tip-in maneuvers were simulated to optimize the PAT valve opening, which is essential to obtain a quick torque increase given the limited amount of pressurized air. The downstream PAT leads to a response time of 0.31 s, slightly faster than in the target tip-in with no EGR. However, its implementation is associated with higher costs and complexity. It requires reducing the EGR rate by partially closing the EGR valve to prevent torque drop after the tank emptying and also defining a strategy to mitigate compressor surge. These two requirements are not needed with the upstream PAT, but the torque response time (0.43 s) is not as fast. Lastly, a tip-in simulation was performed with the electric supercharger system, which was actuated simultaneously with the throttle opening. The e-supercharger reached 48.000 rpm in 0.25 s, providing a time response of 0.41 s while keeping the EGR dilution above 21% during the whole tip-in. This results in a fuel saving of 1.6% regarding the fuel consumed with the downstream PAT.

In short, the fastest torque response is achieved with the downstream PAT, but at the expense of a remarkable increase in complexity, costs, and fuel. The EGR reduction strategy is the simplest solution and leads to an acceptable response time. And the e-supercharger system provides an

excellent tradeoff between torque response and fuel economy.

Credit author statement

José Galindo: Resources, Project administration, Funding acquisition. **Héctor Climent:** Conceptualization, Methodology, Writing - original draft, Writing - review & editing, Supervision. **Joaquín de la Morena:** Methodology, Investigation, Writing - review & editing, Supervision. **David González-Domínguez:** Conceptualization, Methodology, Software, Validation, Formal analysis, Investigation, Writing - original draft, Writing - review & editing. **Stéphane Guilain:** Resources, Writing - review & editing, Funding acquisition.

Declaration of competing interest

The authors declare that they have no known competing financial interests or personal relationships that could have appeared to influence the work reported in this paper.

Data availability

Data will be made available on request.

References

- [1] Burton T, Powers S, Burns C, Conway G, Leach F, Senecal K. A data-driven greenhouse gas emission rate analysis for vehicle comparisons. *SAE Int J Elec Veh* 2023;12. <https://doi.org/10.4271/14-12-01-0006>.
- [2] Qiao Q, Zhao F, Liu Z, Jiang S, Hao H. Comparative study on life cycle CO2 emissions from the production of electric and conventional vehicles in China. *Energy Proc* 2017;105:3584. <https://doi.org/10.1016/j.egypro.2017.03.827>.
- [3] García A, Monsalve-Serrano J, Martínez-Boggio S, Wittek K. Potential of hybrid powertrains in a variable compression ratio downsized turbocharged VVA Spark Ignition engine. *Energy* 2020;195:117039. <https://doi.org/10.1016/j.energy.2020.117039>.
- [4] Huang Y, Surawski NC, Organ B, Zhou JL, Tang OH, Chan EFC. Fuel consumption and emissions performance under real driving: comparison between hybrid and conventional vehicles. *Sci Total Environ* 2019;659:275–82. <https://doi.org/10.1016/j.scitotenv.2018.12.349>.
- [5] Lemazurier L, Shidore N, Kim N, Moawad A, Rousseau A, Bonkoski P, Delhom J. Impact of advanced engine and powertrain technologies on engine operation and fuel consumption for future vehicles. *SAE Tech Pap* 2015. <https://doi.org/10.4271/2015-01-0978>. 2015-01-0978.
- [6] Conway G, Chambon P, Alger T. Opportunities for electrified internal combustion engines. *SAE Tech Pap* 2020. <https://doi.org/10.4271/2020-01-0281>. 2020-01-0281.
- [7] Fraser N, Blaxill H, Lumsden G, Bassett M. Challenges for increased efficiency through gasoline engine downsizing. *SAE Int J Engines* 2009;2:991–1008. <https://doi.org/10.4271/2009-01-1053>.
- [8] Coltman D, Turner JWG, Curtis R, Blake D, Holland B, Pearson RJ, Arden A, Nugglich H. Project sabre: a close-spaced direct injection 3-cylinder engine with synergistic technologies to achieve low CO2 output. *SAE Int J Engines* 2009;1: 129–46. <https://doi.org/10.4271/2008-01-0138>.
- [9] Lumsden G, OudeNijeweme D, Fraser N, Blaxill H. Development of a turbocharged direct injection downsizing demonstrator engine. *SAE Int J Engines* 2009;2: 1420–32. <https://doi.org/10.4271/2009-01-1503>.
- [10] Shahed S, Bauer K. Parametric studies of the impact of turbocharging on gasoline engine downsizing. *SAE Int J Engines* 2009;2:1347–58. <https://doi.org/10.4271/2009-01-1472>.
- [11] Zhao J, Fu R, Wang S, Xu H, Yuan Z. Fuel economy improvement of a turbocharged gasoline SI engine through combining cooled EGR and high compression ratio. *Energy* 2022;239:122353. <https://doi.org/10.1016/j.energy.2021.122353>.
- [12] Alger T, Chauvet T, Dimitrova Z. Synergies between high EGR operation and GDI systems. *SAE Int J Engines* 2009;1:101–14. <https://doi.org/10.4271/2008-01-0134>.
- [13] Luján JM, Climent H, Novella R, Rivas-Perea ME. Influence of a low pressure EGR loop on a gasoline turbocharged direct injection engine. *Appl Therm Eng* 2015;89: 432–43. <https://doi.org/10.1016/j.applthermaleng.2015.06.039>.
- [14] Siokos K, Koli R, Prucka R, Schwanke J, Miersch J. Assessment of cooled low pressure EGR in a turbocharged direct injection gasoline engine. *SAE Int J Engines* 2015;8:1535–43. <https://doi.org/10.4271/2015-01-1253>.
- [15] Potteau S, Lutz P, Leroux S, Moroz S, Tomas E. Cooled EGR for a turbo SI engine to reduce knocking and fuel consumption. *SAE Tech Pap* 2007. <https://doi.org/10.4271/2007-01-3978>. 2007-01-3978.
- [16] Galindo J, Climent H, De la Morena J, Pitarch R, Guilain S, Besançon T. A methodology to study the interaction between variable valve actuation and exhaust gas recirculation systems for spark-ignition engines from combustion

- perspective. *Energy Convers Manag* 2021;250:114859. <https://doi.org/10.1016/j.enconman.2021.114859>.
- [17] Shimura R, Zhao H, Wang X. Expansion of external EGR effective region and influence of dilution on boosted operation of a downsized turbocharged GDI engine. *SAE Tech Pap* 2019. <https://doi.org/10.4271/2019-01-2252>. 2019-01-2252.
- [18] Pilla G, Francqueville L. Stabilization of highly diluted gasoline direct injection engine using innovative ignition systems. *SAE Int J Engines* 2014;7:1734–43. <https://doi.org/10.4271/2014-01-2598>.
- [19] Luján JM, Climent H, Arnau FJ, Miguel-García J. Analysis of low-pressure exhaust gases recirculation transport and control in transient operation of automotive diesel engines. *Appl Therm Eng* 2018;137:184–92. <https://doi.org/10.1016/j.applthermaleng.2018.03.085>.
- [20] Siokos K, Prucka R. Transient operation and over-dilution mitigation for low-pressure EGR systems in spark-ignition engines. *SAE Int J Engines* 2018;11:525–38. <https://doi.org/10.4271/03-11-05-0035>.
- [21] Galindo J, Climent H, de la Morena J, González-Domínguez D, Guilain S, Besançon T. Assessment of air-management strategies to improve the transient performance of a gasoline engine under high EGR conditions during load-decrease operation. *Int J Engine Res* 2021;14680874211055578. <https://doi.org/10.1177/14680874211055578>.
- [22] Zsiga N, Voser C, Onder C, Guzzella L. Intake manifold boosting of turbocharged spark-ignited engines. *Energies* 2013;6:1746–63. <https://doi.org/10.3390/en6031746>.
- [23] Lefebvre A, Guilain S. Transient response of a turbocharged SI engine with an electrical boost pressure supply. *SAE Tech Pap* 2003. <https://doi.org/10.4271/2003-01-1844>. 2003-01-1844.
- [24] Shen K, Xu Z, Zhu Z, Yang L. Combined effects of electric supercharger and LP-EGR on performance of turbocharged engine. *Energy* 2022;244:123176. <https://doi.org/10.1016/j.energy.2022.123176>.
- [25] Galindo J, Climent H, De la Morena J, González-Domínguez D, Guilain S, Besançon T. Experimental and modeling analysis on the optimization of combined VVT and EGR strategies in turbocharged direct-injection gasoline engines with VNT. *Proc Inst Mech Eng - Part D J Automob Eng* 2021;235:2843–56. <https://doi.org/10.1177/09544070211004502>.
- [26] Payri F, Lujan J, Climent H, Pla B. Effects of the intake charge distribution in HSDI engines. *SAE Tech Pap* 2010. <https://doi.org/10.4271/2010-01-1119>. 2010-01-1119.
- [27] Pla B, De La Morena J, Bares P, Jiménez I. Knock analysis in the crank angle domain for low-knocking cycles detection. *SAE Tech Pap* 2020. <https://doi.org/10.4271/2020-01-0549>. 2020-01-0549.
- [28] Pla B, De la Morena J, Bares P, Jiménez I. Cycle-to-cycle combustion variability modelling in spark ignited engines for control purposes. *Int J Engine Res* 2020;21:1398–411. <https://doi.org/10.1177/1468087419885754>.
- [29] Climent H, Dolz V, Pla B, González-Domínguez D. Analysis on the potential of EGR strategy to reduce fuel consumption in hybrid powertrains based on advanced gasoline engines under simulated driving cycle conditions. *Energy Convers Manag* 2022;266:115830. <https://doi.org/10.1016/j.enconman.2022.115830>.
- [30] Serrano J, Climent H, Navarro R, González-Domínguez D. Methodology to standardize and improve the calibration process of a 1d model of a gtdi engine. *SAE Tech Pap* 2020. <https://doi.org/10.4271/2020-01-1008>. 2020-01-1008.
- [31] Lavoie GA, Ortiz-Soto E, Babajimopoulos A, Martz JB, Assanis DN. Thermodynamic sweet spot for high-efficiency, dilute, boosted gasoline engines. *Int J Engine Res* 2013;14:260–78. <https://doi.org/10.1177/1468087412455372>.
- [32] Ghojel JI. Review of the development and applications of the Wiebe function: a tribute to the contribution of Ivan Wiebe to engine research. *Int J Engine Res* 2010;11:297–312. <https://doi.org/10.1243/14680874JER06510>.
- [33] Serrano JR, Arnau FJ, García-Cuevas LM, Gómez-Vilanova A, Guilain S, Batard S. A methodology for measuring turbocharger adiabatic maps in a gas-stand and its usage for calibrating control oriented and one-dimensional models at early ICE design stages. *ASME J Energy Resour Technol* 2021;143:042303. <https://doi.org/10.1115/1.4048229>.
- [34] Broatch A, Diez M, Serrano JR, Olmeda P, Gómez-Vilanova A. An experimental methodology and model for characterizing radial centrifugal compressors of turbocharged engines from diathermal perspective. In: *The 15th IFToMM world Congress on Mechanism and machine science*; 2019. https://doi.org/10.1007/978-3-030-20131-9_88.
- [35] Serrano JR, Arnau FJ, De la Morena J, Gómez-Vilanova A, Guilain S, Batard S. A methodology to calibrate gas-dynamic models of turbocharged petrol engines with variable geometry turbines and with focus on dynamics prediction during tip-in load transient tests. In: *Proceedings of the ASME turbo expo 2020: turbomachinery technical conference and exposition*; 2020. <https://doi.org/10.1115/GT2020-15169>. London, England.
- [36] Galindo J, Climent H, de la Morena J, González-Domínguez D, Guilain S, Besançon T. Compressor surge mitigation in turbocharged spark-ignition engines without an anti-surge control system during load-decrease operation. *Appl Sci* 2022;12:1751. <https://doi.org/10.3390/app12031751>.
- [37] Ossareh HR, Buckland J, Jankovic M. Continuous compressor recirculation to improve boost response and mitigate compressor surge in turbocharged gasoline engines. In: *2016 American control conference (ACC)*; 2016. <https://doi.org/10.1109/ACC.2016.7526161>.